J Therm Anal Calorim (2012) 108:1171–1182
DOI 10.1007/s10973-011-1733-0

The effect of particle size on the thermal decomposition kinetics of potassium bromate

An isothermal thermogravimetric study

V. M. Abdul Mujeeb · K. Muraleedharan · M. P. Kannan · T. Ganga Devi

Received: 6 April 2011 / Accepted: 7 June 2011 / Published online: 24 June 2011

Abstract The thermal decomposition of potassium bromate ($KBrO_3$) has been studied as a function of particle size, in the range 53–150 μm, by isothermal thermogravimetry at different temperatures, viz. 668, 673, 678, and 683 K in static air atmosphere. The theoretical and experimental mass loss data are in good agreement for the thermal decomposition of all samples of $KBrO_3$ at all temperatures studied. The isothermal decomposition of all samples of $KBrO_3$ was subjected to both model fitting and model-free (isoconversional) kinetic methods of analysis. Isothermal model fitting analysis shows that the thermal decomposition kinetics of all the samples of $KBrO_3$ studied can be best described by the contracting square equation. Contrary to the expected increase in rate followed by a decrease with decrease in particle size, $KBrO_3$ shows a regular increase in rate with reduction in particle size, which, we suggest, is an impact of melting of this solid during decomposition.

Keywords Contracting square equation · Effect of particle size · Isothermal thermogravimetry · Potassium bromate · Kinetics and mechanism

V. M. Abdul Mujeeb (✉) · K. Muraleedharan · M. P. Kannan · T. Ganga Devi
Department of Chemistry, University of Calicut, Calicut 673 635, Kerala, India
e-mail: vmamujeeb@gmail.com

K. Muraleedharan
e-mail: kmuralika@gmail.com

Introduction

Potassium bromate ($KBrO_3$) is a white crystalline powder, which is colorless, odorless, and tasteless with a molecular mass of 167 g. It is an oxidizing agent and is typically used as a flour improver, strengthening the dough and allowing higher rising, and under the right conditions, will be completely used up in the baking of bread. However, if too much is added, or if the bread is not baked long enough or not at a high enough temperature, then a residual amount will remain, which may be harmful if consumed. $KBrO_3$ might also be used in the production of malt barley [1]. It has no medicinal value but is added to fish paste as a conditioner, and also to beer or cheese [2]. It has also been used as a constituent in cold wave hair solution [3]. It is a very powerful oxidizer compared to potassium permanganate and is considered a category 2B (possibly carcinogenic to humans) carcinogen by the International Agency for Research on Cancer (IARC) [4]. It has been found that $KBrO_3$ is carcinogenic in rats and nephrotoxic in both man and experimental animals when given orally [5]. In contrast to its weak mutagenic activity in microbial assays, $KBrO_3$ showed relatively strong potential inducing chromosome aberrations both in vitro and in vivo. Glutathione and cysteine degrade $KBrO_3$ in vitro; in turn, the $KBrO_3$ has inhibitory effects on inducing lipid peroxidation in the rat kidney. Active oxygen radicals generated from $KBrO_3$ were implicated in its toxic and carcinogenic effects, especially because $KBrO_3$ produced 8-hydroxydeoxyguanosine in the rat kidney.

$KBrO_3$ may be fatal if swallowed, harmful if inhaled or absorbed through skin and causes irritation to skin, eyes, respiratory tract, and kidney damage. On ingestion, it creates irritation to the gastrointestinal tract; the symptoms include nausea, vomiting, diarrhea, abdominal pain, reduced urinary output and, low blood pressure, methemoglobinemia, convulsions, liver and kidney damage, and coma. Death may occur from renal failure, within 1–2 weeks, the estimated lethal dose is 4 g. It has been known for years that bromate causes cancers in laboratory animals and found to causes tumors of the kidney, thyroid, and other organs in humans. $KBrO_3$ is stable under ordinary conditions of use and storage. It undergoes combustion when in contact with oxidizable substances and explodes when applied shock or friction from mixtures with combustible substances. $KBrO_3$ emits oxygen and toxic fumes of bromine when heated to decomposition.

Thermoanalytical studies

Information about the thermal stability of solid materials of all kinds is of great practical and technological importance [6–8]. Thermogravimetric analysis (TG) is usually adopted to study the kinetics of thermally activated solid-state reactions to obtain thermal stability parameters of solids [9–13]. The kinetics of the thermal decomposition of inorganic materials could be markedly affected by pre-treatments, by the shortening of the induction period followed by an overall decrease in time needed to complete the reaction. The thermal decomposition data generated from TG can be analyzed and manipulated to obtain kinetic parameters such as activation energy (E) and pre-exponential factor (A) [14–16]. Solid-state kinetic data are of practical interest for the large and growing number of technologically important processes. Kinetic studies predict how quickly a system approaches equilibrium and also help to understand the mechanism of the process [17, 18]. A number of reviews are available in the literature on these processes [19–26]. Several authors have emphasized the practical and theoretical importance of information on the kinetics and mechanism of solid-state decompositions [6, 27–29].

The mass loss data obtained from thermogravimetric studies in the present study support the findings of Bancroft and Gesser [30] that the thermal decomposition reaction proceeds according to the equation:

$$2KBrO_3 \rightarrow 2KBr + 3O_2.$$

Jach [31, 32] reported that there is an initial rapid evolution of gas in the thermal decomposition of $KBrO_3$ (1–2% decomposition) which could be eliminated by grinding or irradiation. This initial stage was followed by an exponential decay reaction in the temperature range 615–640 K. At higher temperatures (652–685 K), he observed a short acceleratory process to precede the exponential decay. The activation energies of the acceleratory and decay processes were 171 and 221 kJ mol^{-1}, respectively. He proposed the formation of a eutectic between $KBrO_3$ and the product KBr in order to account for the observed melting of the solid well below the normal melting point, 707 K. According to derivatographic studies, the decomposition of $KBrO_3$ begins after melting, showing endotherms indicating melting at 400 °C and exotherms relating to decomposition at 430 °C [33]. Breusov et al. [34] observed endotherms at 350 °C and exotherms at 405 °C in the differential thermal analysis (DTA) of $KBrO_3$. Solymosi [33] studied the decomposition of $KBrO_3$ in the temperature range 665–677 K and observed that the decomposition obeyed the Prout–Tompkins [35] equation with separate rate constants and activation energies viz., 195 kJ mol^{-1} ($\alpha = 0.04$–0.46) and 173 kJ mol^{-1} ($\alpha = 0.5$–0.95). He also observed that the range $\alpha = 0.3$–0.95 can be fitted to the first-order rate equation with an activation energy of 191.6 kJ mol^{-1}. Diefallah et al. [36] followed the decomposition of $KBrO_3$ by isothermal as well as non-isothermal methods. They reported that under isothermal conditions the kinetics of the decomposition (in the temperature range 653–693 K) followed contracting cube equation with activation energy of 193.3 kJ mol^{-1}.

Joseph et al. [37] investigated catalytic effect of metal oxide on the thermal decomposition of $KBrO_3$ and found that Al_2O_3 is almost as good a catalyst as any other oxide used unlike in the thermal decomposition of $KClO_3$. In the case of TiO_2, there was an increase in the activation energy of decomposition. The effects of admixtures of potassium bromide (2.5 and 5%) on the thermal decomposition of $KBrO_3$ were studied by Mohanty et al. [38], in the temperature range 653–683 K, and found that a three stage process; (i) initial gas evolution, (ii) acceleratory, and (iii) decay steps occurs in the thermal decomposition. They analyzed the TG data on the basis of the first-order law with two rate constants k_1 and k_2, where k_1 being the rate constant for the initial, slow first-order process ($\alpha = 0.02$–0.26), and k_2 being the rate constant for the subsequent faster process in the range $\alpha = 0.21$ to 0.98 and found that the range for the slow and faster processes became 0.01 to 0.16 and 0.1 to 0.98, respectively, when the concentration of added potassium bromide is increased to 5%.

The isothermal decomposition of doped and normal $KBrO_3$ samples was carried out gasometrically between the temperature range 653–663 K, and the results reveal that the process occurs through initial gas evolution, acceleratory, and decay stages [39]. It has also been observed that doping enhances the rate of the reaction, the effect being more pronounced in the case of sulfate, and the TG data were found to be well fitted to the Prout–Tompkins and Avrami–Erofeev mechanisms. It has been found, on survey of the literature, that no more studies on the thermal decomposition and kinetics of potassium bromate are reported in the literature.

Our earlier investigations showed that the isothermal decomposition of $KBrO_3$ proceeds through contracting square model kinetics at all temperatures studied [40, 41].

As a part of our study of the effect of various pretreatments on the thermal behavior of high energy solids, we have examined the isothermal decomposition of $KBrO_3$ as a function of small concentrations of the dopants, SO_4^{2-} & Ba^{2+} [40] and PO_4^{3-} & Al^{3+} [41], by isothermal thermogravimetry in the temperature range 668–683 K. The results suggested a diffusion-controlled mechanism for the decomposition of $KBrO_3$, the diffusing species being both K^+ and BrO_3^-. Pure and doped samples of $KBrO_3$ were subjected to pre-compression, and their thermal decomposition kinetics was studied by TG at 668 K [42]. The samples decomposed in two stages governed by the same rate law (contracting square equation), but with different rate constants, k_1 (for $\alpha \leq 0.45$) and k_2 (for $\alpha \geq 0.45$), as in the case of uncompressed samples. The rate constants k_1 and k_2 decreased dramatically on pre-compression, the decrease being higher for doped samples. The effects caused by cation dopants (Ba^{2+} & Al^{3+}) are more than that of the anion dopants (SO_4^{2-} & PO_4^{3-}) of the same magnitude of charge and concentration. The results favor ionic diffusion mechanism proposed earlier on the basis of doping studies [40, 41].

The objective of this study is to investigate the effect of particle size on the thermal decomposition kinetics of $KBrO_3$ by isothermal thermogravimetry. In the present study, great emphasis is given to reliable activation energy values for the forward reaction, $2KBrO_3 \rightarrow 2KBr + 3O_2$, which allows one to draw mechanistic conclusions as well as to predict the kinetics of the process.

Experimental

Materials

AnalaR grade $KBrO_3$ of E Merck is dissolved in water, recrystalized, dried, and kept in a vacuum desiccator. To study the effect of *particle size*, recrystalized $KBrO_3$ sample was powdered in an agate mortar, sieved into six different particle size ranges, viz., 53–63, 63–75, 75–90, 90–106, 106–125, and 125–150 µm, and kept in a vacuum desiccator.

Methods

Thermogravimetric measurements in static air were carried out on a custom-made thermobalance fabricated in this laboratory [43]. A major problem [44] of the isothermal experiment is that a sample requires some time to reach the experimental temperature. During this period of non-isothermal heating, the sample undergoes some transformations that are likely to affect the succeeding kinetics. The situation is especially aggravated by the fact that under isothermal conditions, a typical solid-state process has its maximum reaction rate at the beginning of the transformation. Therefore, we fabricated a thermobalance particularly for isothermal studies, in which loading of the sample is possible at any time after the furnace has attained the desired reaction temperature. The operational characteristics of the thermobalance are, balance sensitivity: $\pm 1 \times 10^{-5}$ g, temperature accuracy: $\pm$ 0.5 K, sample mass: 5×10^{-2} g, atmosphere:

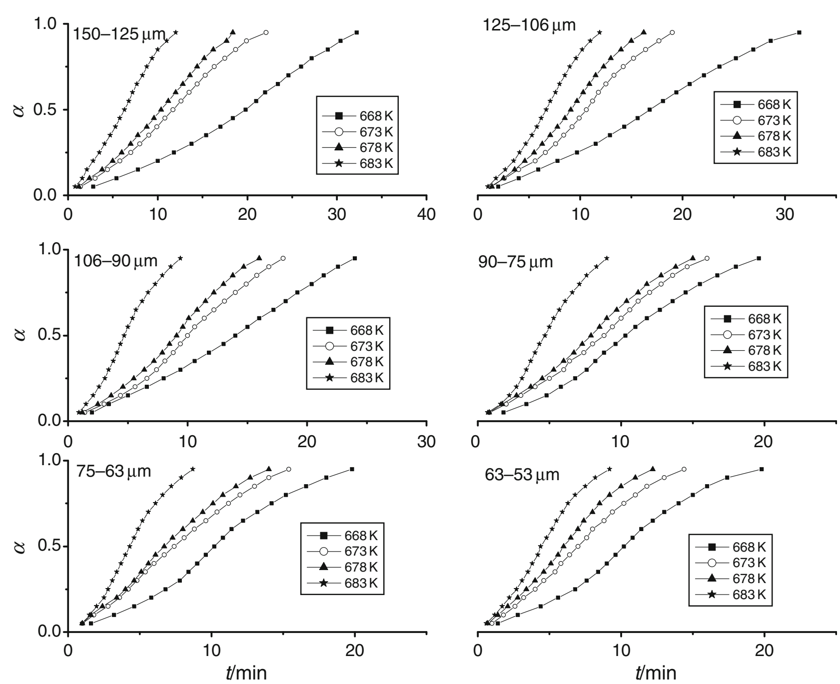

Fig. 1 α versus *t* curves for the thermal decomposition of all samples of $KBrO_3$ at all temperatures studied

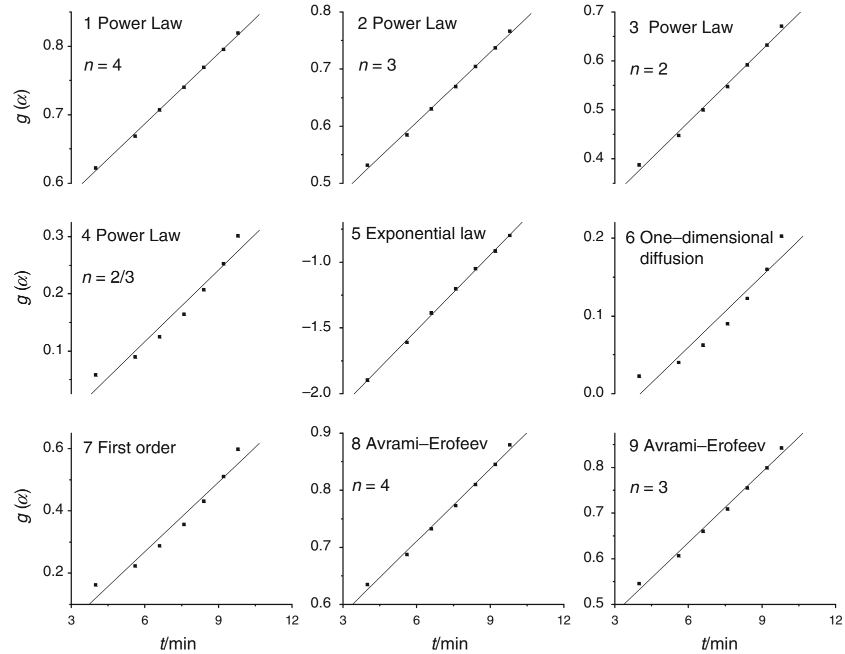

Fig. 2 Typical model fitting plots (models 1–9) for the thermal decomposition of $KBrO_3$ (particle size; 125–106 μm) in the range $\alpha = 0.15–0.45$ at 673 K

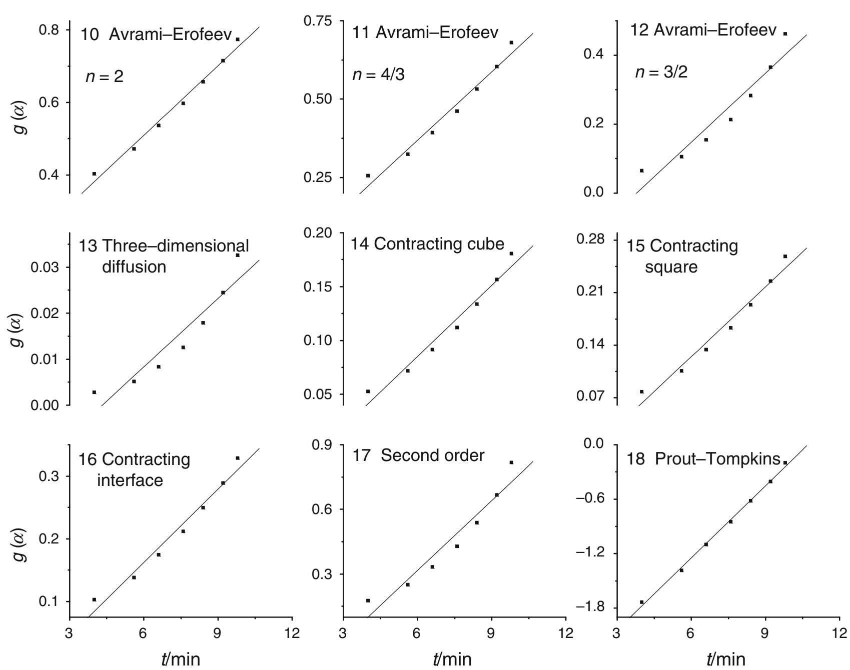

Fig. 3 Typical model fitting plots (models 10–18) for the thermal decomposition of $KBrO_3$ (particle size; 125–106 μm) in the range $\alpha = 0.15–0.45$ at 673 K

static air, and crucible: platinum. Comparative runs were always made using samples of same age and particle size. The fraction of solid decomposed (α) was measured as a function of time (t) at four temperatures (T), viz., 668, 673, 678, and 683 K for all samples of $KBrO_3$.

Calculation of fractional decomposition, α

On the assumption that both solid and gaseous products maintain a constant composition, the conventional dimensionless fractional decomposition, α, at any time during the thermal decomposition is measured directly from the mass loss at that time relative to the overall mass loss when decomposition is complete. Thus, the TG mass loss data are transformed into α using the following relation:

$$\alpha = (m_0 - m_t)/(m_0 - m_f),$$

where m_0 is the initial mass of reactant, m_t is the mass of the reactant at time, t, and m_f is the mass of the residue at infinite time.

Table 1 Values of slope and correlation coefficient (r) obtained from model fitting to different kinetic equations for the thermal decomposition region; $\alpha = 0.15$–0.45 at 673 K

Model no.	Particle size/μm											
	150–125		125–106		106–90		90–75		75–63		63–53	
	Slope	r	Slope	r	Slope	r	Slope	r	Slope	r	Slope	r
1	0.0351	0.9988	0.0341	0.9993	0.0378	0.9967	0.0390	0.9973	0.0472	0.9941	0.0503	0.9958
2	0.0420	0.9983	0.0408	0.9988	0.0452	0.9968	0.0466	0.9977	0.0564	0.9953	0.0602	0.9967
3	0.0506	0.9965	0.0492	0.9974	0.0546	0.9986	0.0563	0.9980	0.0683	0.9973	0.0728	0.9979
4	0.0430	0.9735	0.0418	0.9763	0.0467	0.9852	0.0484	0.9861	0.0592	0.9954	0.0628	0.9909
5	0.1959	0.9976	0.1904	0.9996	0.2103	0.9981	0.2168	0.9950	0.2616	0.9893	0.2793	0.9920
6	0.0313	0.9558	0.0305	0.9595	0.0342	0.9712	0.0354	0.9732	0.0436	0.9872	0.0461	0.9798
7	0.0764	0.9763	0.0744	0.9789	0.0830	0.9872	0.0859	0.9879	0.1052	0.9965	0.1115	0.9920
8	0.0435	0.9965	0.0423	0.9975	0.0469	0.9976	0.0484	0.9980	0.0587	0.9974	0.0625	0.9977
9	0.0527	0.9952	0.0513	0.9963	0.0569	0.9982	0.0588	0.9978	0.0714	0.9983	0.0760	0.9981
10	0.0656	0.9918	0.0639	0.9933	0.0710	0.9975	0.0733	0.9967	0.0892	0.9932	0.0949	0.9981
11	0.0749	0.9849	0.0729	0.9870	0.0811	0.9933	0.0839	0.9933	0.1024	0.9989	0.1087	0.9961
12	0.0684	0.9546	0.0668	0.9583	0.0748	0.9701	0.0775	0.9722	0.0954	0.9866	0.1008	0.9785
13	0.0051	0.9386	0.0050	0.9429	0.0056	0.9567	0.0058	0.9596	0.0072	0.9773	0.0075	0.9671
14	0.0226	**0.9998**	0.0220	**0.9996**	0.0245	**0.9992**	0.0253	**0.9996**	0.0310	**0.9998**	0.0329	**0.9994**
15	0.0319	0.9982	0.0310	0.9990	0.0346	0.9986	0.0358	0.9989	0.0437	0.9993	0.0464	0.9989
16	0.0400	0.9842	0.0390	0.9863	0.0434	0.9928	0.0449	0.9929	0.0548	0.9987	0.0582	0.9960
17	0.1108	0.9614	0.1080	0.9648	0.1208	0.9755	0.1252	0.9773	0.1539	0.9901	0.1627	0.9828
18	0.2723	0.9978	0.2648	0.9985	0.2933	0.9978	0.3027	0.9978	0.3668	0.9962	0.3908	0.9969

Bold value indicates the maximum correlation coefficient obtained

Calculation of average particle size

The average particle size of the grains was calculated according to the Andreasen [45] method:

$$d_{\text{mean}} = \left\{2d_b^2 d_m^2/[d_b + d_m]\right\}^{(1/3)},$$

where d_b and d_m are, respectively, the largest and smallest diameters corresponding to the width of the apertures of coarser and finer screens, and d_{mean} is the average diameter of the grains/particles.

Results and discussion

The experimental mass loss data obtained from TG were transformed into α versus t data, in the range $\alpha = 0.05$–0.95 with an interval of 0.05, for all the samples studied. The α versus t curves for the isothermal decomposition, at different temperatures, of all samples of $KBrO_3$ studied are shown in Fig. 1. The observed mass changes for the decomposition agree very well with the theoretical value for all samples of $KBrO_3$ at all temperatures studied.

Model fitting method

The α versus t data in the range $\alpha = 0.05$–0.95 of the isothermal decomposition of all samples of $KBrO_3$ were subjected to weighted least squares analysis to various kinetic models [41] as described earlier [46]. We observed that no single equation fitted the whole α versus t data with a single rate constant throughout the reaction. Separate kinetic analysis shows that the decomposition proceeded through two stages: a slow reaction ($\alpha = 0.15$–0.45) described by *contracting square equation*[1] $[1 - (1 - \alpha)^{1/2} = kt]$ with rate constant k_1 followed by a faster reaction ($\alpha = 0.5$–0.95) described by *contracting square equation* itself, but with a larger rate constant k_2. The rate law envisages two-dimensional phase boundary reaction. Particle sizing did not affect the rate law of these two stages of decomposition. Typical model fitting plots for various models for the thermal decomposition of $KBrO_3$ in the ranges $\alpha = 0.15$–0.45 and 0.05–0.95 at 673 K are shown in Figs. 2 and 3. Similar model fits were obtained for all other samples at all ranges of α and at all temperatures studied (not shown).

[1] Contracting square and contracting cube model equations: For crystals with instantaneous nucleation over all the surface, the nucleus growth takes place inwards to the centre of the crystal and the rate will be deceleratory throughout the process as the interface area will be decreasing progressively. The growth of the product inwards is considered to take place in different manners. In contracting cube model, the inward growth of the product will be considered in the form of a cube, while in contracting square model it is considered on the basis of decreasing interfacial contact area.

Table 2 Values of slope and correlation coefficient (*r*) obtained from model fitting to different kinetic equations for the thermal decomposition region; $\alpha = 0.5$–0.95 at 673 K

Model no.	Particle size/μm											
	150–125		125–106		106–90		90–75		75–63		63–53	
	Slope	*r*	Slope	*r*	Slope	*r*	Slope	*r*	Slope	*r*	Slope	*r*
1	0.0162	0.9747	0.0156	0.9735	0.0182	0.9885	0.0205	0.9805	0.0187	0.9847	0.0197	0.9769
2	0.0210	0.9762	0.0202	0.9750	0.0235	0.9896	0.0266	0.9819	0.0243	0.9859	0.0256	0.9784
3	0.0298	0.9792	0.0286	0.9777	0.0333	0.9916	0.0377	0.9845	0.0344	0.9883	0.0363	0.9813
4	0.0649	0.9926	0.0622	0.9890	0.0722	0.9989	0.0819	0.9955	0.0746	0.9975	0.0790	0.9938
5	0.0705	0.9696	0.0678	0.9689	0.0792	0.9850	0.0894	0.9761	0.0816	0.9806	0.0860	0.9721
6	0.0744	0.9965	0.0712	0.9915	0.0825	0.9986	0.0938	0.9982	0.0853	0.9993	0.0905	0.9972
7	0.2451	0.9874	0.2299	0.9624	0.2673	0.9737	0.3077	0.9840	0.2781	0.9791	0.2978	0.9862
8	0.0439	0.9992	0.0417	0.9851	0.0485	0.9972	0.0554	0.9996	0.0502	0.9987	0.0534	0.9995
9	0.0606	0.9992	0.0574	0.9840	0.0667	0.9958	0.0763	0.9992	0.0692	0.9978	0.0737	0.9993
10	0.0974	0.9981	0.0921	0.9807	0.1070	0.9921	0.1225	0.9972	0.1110	0.9949	0.1184	0.9979
11	0.1632	0.9941	0.1538	0.9730	0.1787	0.9842	0.2051	0.9919	0.1856	0.9883	0.1984	0.9934
12	0.4775	0.9672	0.4437	0.9339	0.5166	0.9464	0.5979	0.9616	0.5389	0.9543	0.5794	0.9652
13	0.0381	0.9810	0.0357	0.9550	0.0414	0.9643	0.0478	0.9764	0.0431	0.9706	0.0463	0.9793
14	0.0467	**0.9998**	0.0442	**0.9993**	0.0513	**0.9991**	0.0587	**0.9997**	0.0532	**0.9995**	0.0567	**0.9994**
15	0.0536	0.9991	0.0510	0.9988	0.0592	0.9988	0.0676	0.9988	0.0613	0.9989	0.0652	0.9987
16	0.0552	0.9975	0.0527	0.9896	0.0612	0.9978	0.0697	0.9991	0.0633	0.9988	0.0672	0.9982
17	1.6644	0.8862	1.4970	0.8283	1.7695	0.8522	2.0760	0.8776	1.8587	0.8651	2.0169	0.8831
18	0.3157	0.9969	0.2978	0.9771	0.3465	0.9896	0.3971	0.9957	0.3597	0.9929	0.3837	0.9965

Bold value indicates the maximum correlation coefficient obtained

Table 3 Values of rate constant k_1 and k_2 obtained from model fitting to contracting square equation for all samples of $KBrO_3$ at different temperatures

Rate constant	Particle size/μm	Temperature/K			
		668	673	678	683
k_1/min^{-1}	150–125	0.0120	0.0206	0.0221	0.0343
	125–106	0.0134	0.0220	0.0251	0.0361
	106–90	0.0150	0.0245	0.0264	0.0404
	90–75	0.0267	0.0263	0.0277	0.0439
	75–63	0.0272	0.0310	0.0328	0.0487
	63–53	0.0282	0.0329	0.0364	0.0513
k_2/min^{-1}	150–125	0.0303	0.0367	0.0486	0.0701
	125–106	0.0333	0.0412	0.0527	0.0755
	106–90	0.0371	0.0468	0.0572	0.0801
	90–75	0.0398	0.0507	0.0608	0.0865
	75–63	0.0428	0.0532	0.0637	0.0909
	63–53	0.0447	0.0567	0.0684	0.0942

The values of slope and correlation coefficient (*r*) obtained by weighted least squares plot for the isothermal decomposition of $KBrO_3$ at 673 K for all kinetic models studied are given in Tables 1 and 2. Perusal of Tables 1 and 2 and Figs. 2 and 3 shows that the contracting square equation, $1-(1-\alpha)^{1/3}=kt$, gave the best fits ($r > 0.999$) at all temperatures studied. Similar results were obtained for all other samples and at all temperatures studied.

Separate kinetic analysis of the α versus t data corresponding to the ranges, $\alpha = 0.15$–0.45 and $\alpha = 0.5$–0.95, showed that the both ranges gave the best fits to contracting square model but with different rate constants, k_1 and k_2.

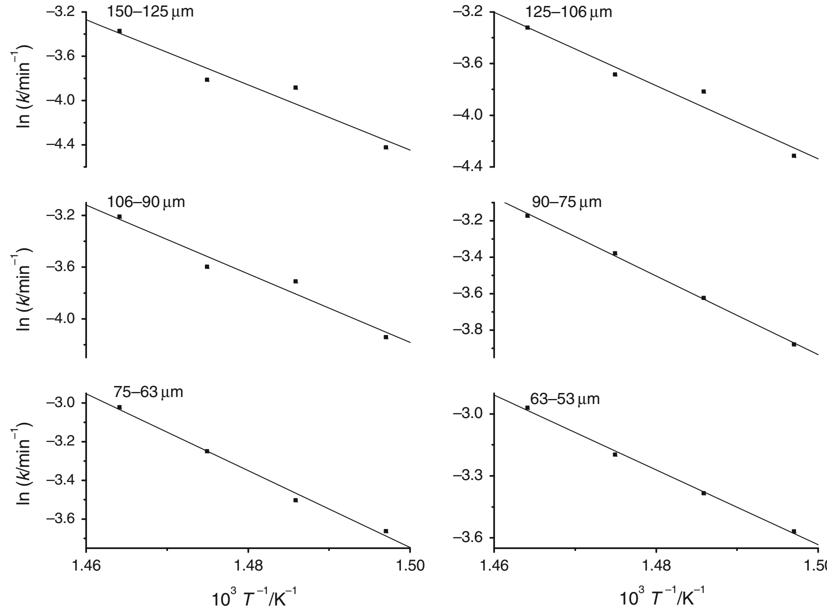

Fig. 4 Arrhenius plots (for the range, $\alpha = 0.15$–0.45 to the contracting square model) for the isothermal decomposition of all samples of $KBrO_3$

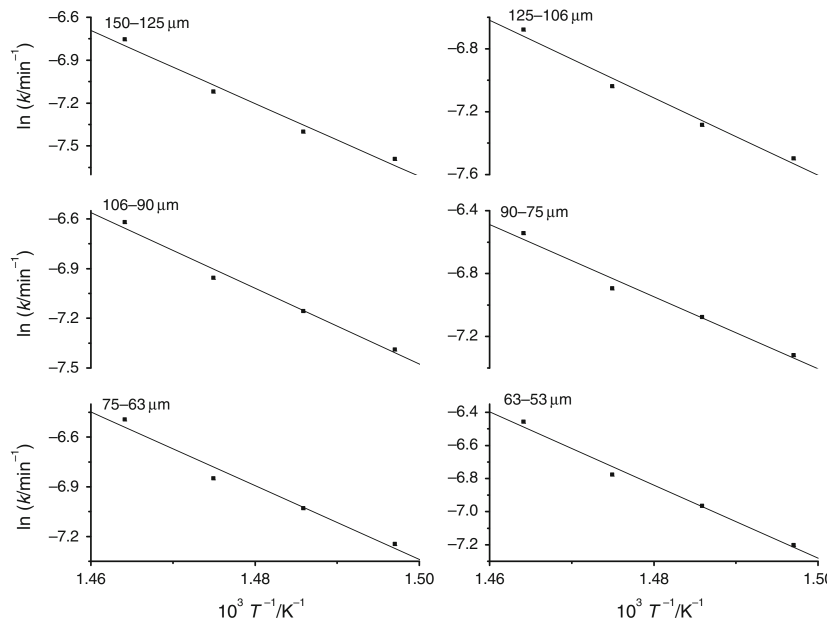

Fig. 5 Arrhenius plots (for the range, $\alpha = 0.5$–0.95 to the contracting square model) for the isothermal decomposition of all samples of $KBrO_3$

Table 4 Values of *E* and *r* obtained through model fitting to contracting square equation for different ranges of the thermal decomposition of all samples of $KBrO_3$

Particle size/µm	Range 1 ($\alpha = 0.15$–0.45)		Range 2 ($\alpha = 0.5$–0.95)	
	E/kJ mol^{-1}	*r*	*E*/kJ mol^{-1}	*r*
150–125	244.5	−0.9659	212.0	−0.9895
125–106	235.7	−0.9784	204.8	−0.9915
106–90	220.8	−0.9793	190.3	−0.9929
90–75	212.4	−0.9992	190.3	−0.9904
75–63	206.2	−0.9954	184.9	−0.9876
63–53	191.9	−0.9984	183.8	−0.9938

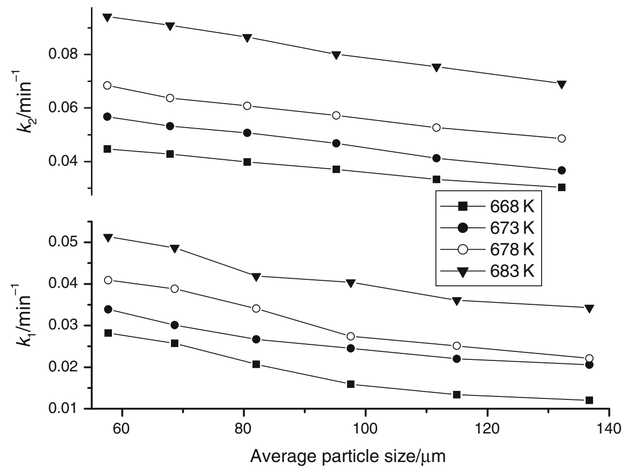

Fig. 6 Plot of average particle size against rate constant (k_1 and k_2) at different temperatures

Description of reaction kinetics using different rate constants for different ranges of α is not unusual in solid-state reactions. For instance, the acceleratory and decay regions of the thermal decomposition of sodium perchlorate and of potassium bromate were well described by the Prout–Tompkins relation with separate rate constants [33]. Mohanty et al. [38] reported that the thermal decomposition of $KBrO_3$ mixed with potassium bromide (2.5–5%) followed the first-order rate law with two rate constants k_1 and k_2, k_1 being the rate constant for the initial, slow process ($\alpha = 0.02$–0.26), and k_2 being the rate constant for the subsequent faster process in the range $\alpha = 0.21$ to 0.98. It has also been reported that $KBrO_3$ decomposes in two stages, both stages following the contracting square equation but with different rate constants [40, 41]. Similarly, several authors described the solid-state reaction kinetics using different rate laws for different ranges of α [46–52]. Philips and Taylor used Prout–Tompkins equation to describe the acceleratory region of the decomposition of KIO_4 and the contracting cube equation for the decay stage [47]. It has also been reported that under isothermal conditions KIO_4 decomposes via two stages; the Prout–Tompkins equation best describes the acceleratory stage and the deceleratory stage proceeds according to contracting area law [48–50]. The acceleratory stage in the decomposition of Lithium perchlorate followed Prout–Tompkins rates law, whereas the decay stage followed the monomolecular model [51]. Kim et al. [52] have reported that the reaction model varies with reaction temperature in isothermal pyrolysis of polypropylene and they observed that the Arrhenius parameters derived from the assumptions of *n*th order model would be improper. We found that the contracting cube and contracting square models gave best fits to the α versus *t* data of the thermal decomposition of potassium iodate corresponding to the range $\alpha = 0.05$–0.5, while the other range ($\alpha > 0.5$) best describes to the contracting cube model [47].

The values of rate constant (both k_1 and k_2) for the thermal decomposition of all samples $KBrO_3$ and at all temperatures studied are given in Table 3. The Arrhenius plots (for both ranges, $\alpha = 0.15$–0.45 and $\alpha = 0.5$–0.95, to the contracting square model) for the isothermal decomposition of all samples of $KBrO_3$ are shown in Figs. 4 and 5. Values of *E* and correlation coefficient (*r*) obtained from the Arrhenius plots for both ranges of α are given in Table 4. We found that the activation energy values

Fig. 7 Typical isoconversional plots for the thermal decomposition of $KBrO_3$ (particle size; 125–106 µm) at different conversions

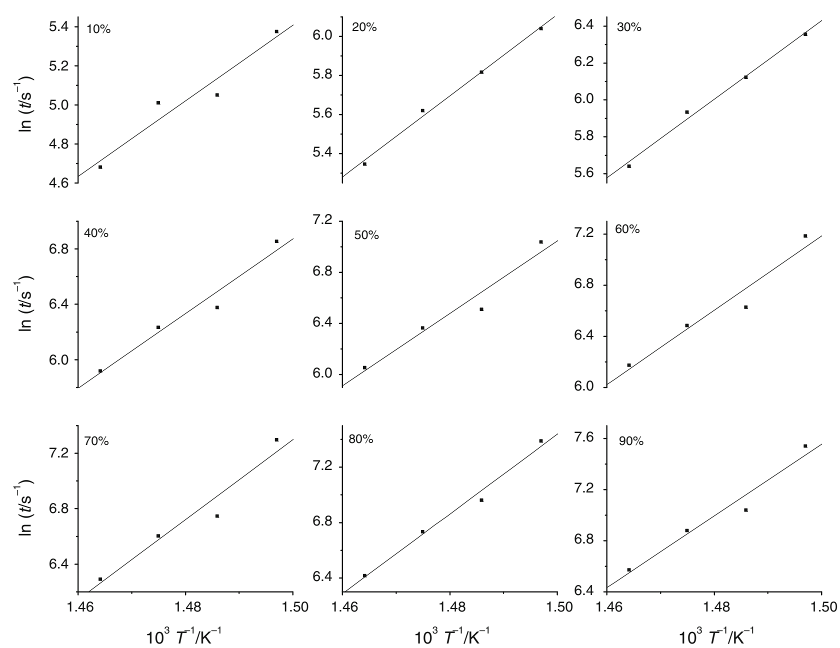

Table 5 Values of activation energy (in kJ mol^{-1}) obtained through isoconversional method for the thermal decomposition of all samples of $KBrO_3$ at different conversions

Conversion/%	Particle size/µm					
	150–125	106–125	90–106	75–90	75–63	63–53
5	293.1	220.6	222.6	220.1	177.5	215.7
10	294.0	215.3	238.5	212.2	180.1	184.4
15	292.8	210.9	224.8	233.0	189.7	185.8
20	290.4	223.8	215.3	223.1	191.7	180.0
25	288.3	225.5	217.2	222.9	200.2	186.7
30	286.4	229.8	214.2	215.0	210.0	192.2
35	277.6	231.1	208.3	211.6	199.2	185.7
40	270.4	240.9	209.9	206.2	197.4	186.6
45	266.0	246.9	223.9	198.4	191.3	189.3
50	263.6	245.9	229.0	203.1	190.1	184.1
55	258.1	246.1	235.2	196.5	189.1	186.7
60	255.5	243.9	238.8	188.8	183.8	189.7
65	254.2	246.1	241.5	194.5	187.7	186.9
70	247.4	245.7	242.4	192.0	190.7	184.3
75	246.7	245.6	240.0	195.6	193.3	182.4
80	243.9	242.3	239.9	193.6	190.8	182.0
85	245.1	236.4	239.0	185.0	188.6	182.0
90	241.3	229.8	237.8	183.9	183.4	180.1
95	239.5	222.0	233.1	187.1	207.5	181.7
Average value of *E*	**266.0**	**234.1**	**229.0**	**203.3**	**191.7**	**186.6**

Bold values are average *E* obtained for a particular sample of $KBrO_3$

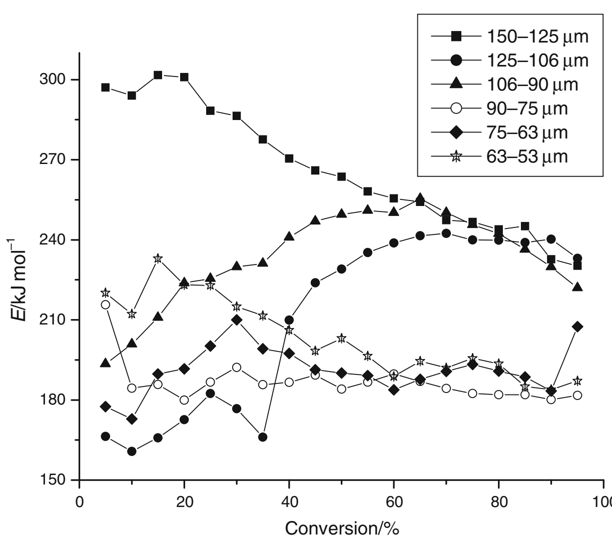

Fig. 8 Dependence of *E* (obtained through model free method) on conversion for all samples of $KBrO_3$

obtained for the different ranges of α remains within 218 ± 26.5 and 198 ± 14.2 kJ mol^{-1}, respectively, for the decomposition ranges $\alpha = 0.15$–0.45 and $\alpha = 0.5$–0.95.

The results presented in Table 3 show that the rate is strongly dependent on particle size; it increases as the particle size decreases (i.e., with an increase in the surface area). This behavior is shown in Fig. 6 where the rate of reaction is plotted against the average particle size of the grains, calculated according to the Andresaen method [45]. A similar effect has been reported in the thermal decomposition of NaN_3 [53], potassium iodate [46], and in the thermal decomposition [54] and sublimation [55] of ammonium perchlorate. It has been shown by several authors that particle size is an important factor in the kinetics of the thermal decomposition of solids [53–60]. Huang et al. [61] have studied the effect of particle size on combustion of aluminum particle dust in air and observed that the particle burning time is size dependent. Chou and Olsen [62] found an unusual dependence of rate on particle size in the thermal decomposition of isothiocynatopentaammine cobalt(III) perchlorate. They observed that when α was less than 0.09, the larger particles decomposed relatively rapidly with an activation energy value of 138 kJ mol^{-1}, and thereafter the reaction rate decreased and the decomposition proceeds with activation energy values in between 88 and 117 kJ mol^{-1}.

Model free method

The α versus t data, in the range of $\alpha = 0.05$–0.95, of the isothermal decomposition of $KBrO_3$ were also subjected to isoconversional studies for the determination of apparent activation energy as a function of α from the sets of isothermals obtained [46]. A plot of ln t (t being the time required for reaching a given value of α at a constant temperature T) versus the corresponding reciprocal of the temperature ($1/T$) would lead to the activation energy for the given value of α. Typical isoconversional plots for the isothermal decomposition of $KBrO_3$ (particle size: 106–125 μm) are shown in Fig. 7. Similar plots were obtained for all other samples and at all conversions studied (not shown). The values of activation energy obtained for the thermal decomposition of all samples $KBrO_3$ at different conversions are given in Table 5, and the dependence of E on conversion is shown in Fig. 8. A perusal of Tables 4 and 5 reveals that the E values obtained for all $KBrO_3$ samples from model fitting and model-free methods are in good agreement.

It is well known that the gross imperfections are present more on the surface than in the bulk [55]. When the particle size is decreased, the surface area increases which in turn results in an increase in the concentration of gross imperfections. The larger the concentration of gross imperfections, the greater the number of nuclei formed [54] leading to an enhancement in the rate of decomposition. The thermal decomposition of solids in which the rate increases by decreasing the particle size [54] has been explained on the basis of Mampel's theory. Mampel's theory is concerned with nucleation and growth in systems consisting of microcrystals in the form of spheres, and theoretically Mampel has shown that the isothermal decomposition rate of a solid should increase because, as the particle size is decreased (i.e., when the surface area is increased), the number of surface defects, which can act as potential nucleus forming sites, increases leading to an enhanced nucleation and growth, or in other words, a sensitization in the rate of decomposition.

Thus, the rate of reaction of a solid is expected to increase with decrease in particle size. Experimentally, this has been found to be true in many systems, but only up to a critical value of the particle size. A further decrease beyond the critical size, however, led to a decrease of rate rather than an increase as found by several authors [55, 56, 60]. Contrary to the above, in the present system of $KBrO_3$, we observed a steady increase in the rate of the decomposition (both stages) with decrease in particle size. The absence of a maximum in the rate versus particle size plot is associated with the formation of KBr–$KBrO_3$ eutectic and consequent melting of the system. Several authors reported this type of phenomena, formation of KBr–$KBrO_3$ eutectic and consequent melting of the system, in the thermal decomposition of $KBrO_3$ [31, 32, 38]. When the size of the particles decreases, the number of potential sites increases, as stated above, resulting in an easy formation of the product nuclei. Thus, more and more KBr species will be formed, which diffuse into the host $KBrO_3$ eutectic at more and more regions. Formation of eutectic leads to localized melting thereby augmenting the diffusion of K^+ and BrO_3^- in the lattice and hence the reaction rate [41].

Conclusions

The importance of surface in solid-state reactions is illustrated in the study of the decomposition reaction as a function of particle size. The present study showed that in the isothermal decomposition of $KBrO_3$, the rate increases as the particle size decreases; the mechanism of the reaction, contracting square equation, remains the same with different rate constants. We suggest that the observed steady increase in the rate of the decomposition of both stages with decrease in particle size is associated with the formation of KBr–$KBrO_3$ eutectic and consequent melting of the system. When the size of the particles decreases, the number of potential sites increases, resulting in an easy formation of the product nuclei. Thus, more and more KBr species will be formed, which diffuse into the host $KBrO_3$ eutectic at more and more regions. Formation of eutectic leads to localized melting thereby augmenting the diffusion of K^+ and BrO_3^- in the lattice and hence the reaction rate. This study demonstrates how strongly the particle size of the sample influences the reactivity of $KBrO_3$ providing information to the solid-state reactivity database.

The results from isoconversional studies on the thermal decomposition reaction shows non-consistent values of E for the entire range of particle size studied. This is expected as the thermal decomposition reaction of $KBrO_3$ follows through different ranges of α with different rate constants. The high values of activation energy values observed in the present study are generally characteristic of the decomposition reactions of metal oxy halides. The initial step in the thermal decomposition is the rupture of a Br–O bond, and the energy barrier to the reactions is not very sensitive to the properties of the cation present.

References

1. Section 172.730 Potassium bromate. Food additives permitted for direct addition to food for human consumption, US Code of Federal Regulations. US Food and Drug Administration.
2. Chipman JK, Davies JE, Parson JL, O'Neill G, Fawell JK. DNA oxidation by potassium bromate; a direct mechanism or link to lipid peroxidation? Toxicology. 1988;126:93–102.

3. Ueno H, Oishi K, Sayato Y, Nakamuro K. Oxidative cell damage in kat-sod assay of oxyhalides as inorganic disinfection by products and their occurrence by ozonation. Arch Environ Contam Toxicol. 2000;38:1–6.
4. IARC-Summaries & Evaluations: Potassium bromate (Group 2B), International Agency for Research on Cancer.
5. Kurokawa Y, Maekawa A, Takahashi M, Hayashi Y. Toxicity and carcinogenicity of potassium bromate—a new renal carcinogen. Environ Health Perspect. 1990;87:309–35.
6. Galwey AK, Brown ME. Thermal decomposition of ionic solids. Amsterdam: Elsevier; 1999.
7. Stern KH. High temperature properties and thermal decomposition of inorganic salts with oxy anions. Florida: CRC Press LLC; 2001.
8. Vyazovkin S. Thermal analysis. Anal Chem. 2004;76:3299–312.
9. Deng C, Cai J, Liu R. Kinetic analysis of solid state reactions: evaluation of approximations to temperature integral and their applications. Solid State Sci. 2009;11:1375–9.
10. Vecchio S, Rodante F, Tomassetti M. Thermal stability of disodium and calcium phosphomycin and the effects of the excipients evaluated by thermal analysis. J Pharm Biomed Anal. 2001;24:1111–23.
11. Huang Y, Cheng Y, Alexander K, Dollimore D. The thermal analysis study of the drug captopril. Thermochim Acta. 2001;367:43–58.
12. Dollimore D, O'Connell C. A comparison of the thermal decomposition of preservatives, using thermogravimetry and rising temperature kinetics. Thermochim Acta. 1998;324:33–48.
13. Halikia I, Neou-Syngouna P, Kolitsa D. Isothermal kinetic analysis of the thermal decomposition of magnesium hydroxide using thermogravimetric data. Thermochim Acta. 1998;320:75–88.
14. Vyazovkin S, Wight CA. Model-free and model-fitting approaches to kinetic analysis of isothermal and nonisothermal data. Thermochim Acta. 1999;340–341:53–68.
15. Rodante F, Vecchio S, Tomassetti M. Kinetic analysis of thermal decomposition for penicillin sodium salts: model-fitting and model-free methods. J Pharm Biomed Anal. 2002;29:1031–43.
16. Brown ME. Introduction to thermal analysis: techniques and applications. 2nd ed. The Netherlands: Kluwer Academic Publishers; 2001.
17. Malek J, Mitsuhashi T, Criado M. Kinetic analysis of solid-state processes. J Mater Res. 2001;16:1862–71.
18. Zhou D, Schmitt EA, Zhang GG, Law D, Vyazovkin S, Wight CA, Grant DJW. Crystallization kinetics of amorphous nifedipine studied by model-fitting and model-free approaches. J Pharm Sci. 2003;92:1779–91.
19. Benderskii VA, Makarov DE, Wight CA. Chemical dynamics at low temperatures. New York: Wiley; 1994. p. 385.
20. Brown ME, Dollimore D, Galwey AK. Reactions in the solid state, comprehensive chemical kinetics, vol. 22. Amsterdam: Elsevier; 1980. p. 340.
21. Vyazovkin S, Wight CA. Isothermal and nonisothermal reaction kinetics in solids: in search of ways toward consensus. J Phys Chem. 1997;101A:8279–84.
22. Brill TB, James KJ. Kinetics and mechanisms of thermal decomposition of nitroaromatic explosives. Chem Rev. 1993;93:2667–92.
23. Mark HF, Bikales NM, Overberger CG, Menges G, editors. Encyclopedia of polymer science and engineering. New York: Wiley; 1989. p. 231, 690.
24. Vyazovkin S, Wight CA. Isothermal and nonisothermal kinetics of thermally stimulated reactions of solids. Int Rev Phys Chem. 1998;17:407–33.
25. Dollimore D. Thermal analysis. Chem Rev. 1996;68:63–72.
26. Galwey AK. Is the science of thermal analysis kinetics based on solid foundations? A literature appraisal. Thermochim Acta. 2004;413:139–83.
27. Vyazovkin S. Kinetic concepts of thermally stimulated reactions in solids: a view from a historical perspective. Int Rev Phys Chem. 2000;19:45–60.
28. Kotler JM, Hinman NW, Richardson CD, Scott JR. J Therm Anal Calorim. 2010;102:23–9.
29. Bertol CD, Cruz AP, Stulzer HK, Murakami FS, Silva MAS. Thermal decomposition behaviour of potassium and sodium jasorite synthesized in the presence of methyl amine and alanine. J Therm Anal Calorim. 2010;102:187–92.
30. Bancroft GM, Gesser HD. The search for perbromate. I: The thermal decomposition of bromates. J Inorg Nucl Chem. 1965;27:1545–56.
31. Jach J. Decomposition of metal perhalates, halates and halites. In: de Boer JH, editors. Reactivity of solids. Amsterdam: Elsevier; 1960. p. 334.
32. Jach J. The thermal decomposition of $NaBrO_3$ part I—unirradiated material. J Phys Chem Solids. 1963;24:63–73.
33. Solymosi F. Structure and stability of salts of halogen oxyacids in the solid phase. London: John Wiley & Sons; 1977.
34. Breusov CN, Kashina NI, Revzina TV. Thermal decomposition of chlorates, bromates, iodates, perchlorates and periodates of potassium, rubidium and cesium. Zh Neorg Khim. 1970;15:612–24.
35. Prout EG, Tompkins FC. The thermal decomposition of potassium permanganate. Trans Faraday Soc. 1944;40:488–97.
36. Diefallah EM, Basahl SN, Obaid AY, Abu-Eittah RH. Kinetic analysis of thermal decomposition reactions: I. Thermal decomposition of potassium bromate. Thermochim Acta. 1987;111:49–56.
37. Joseph J, Nair TDR. Effect of metal oxide catalysts on thermal decomposition of potassium bromate. J Therm Anal Calorim. 1978;14:271–9.
38. Mohanty SR, Patnaik D. Effects of admixtures of potassium bromide on the thermal decomposition of potassium bromate. J Therm Anal Calorim. 1989;35:2153–9.
39. Das BC, Patnaik D. Effect of anion doping on the thermal decomposition of potassium bromate. J Therm Anal Calorim. 2000;61:879–83.
40. Kannan MP, Abdul Mujeeb VM. Effect of dopant ion on the kinetics of thermal decomposition of potassium bromate. React Kinet Catal Lett. 2001;72:245–52.
41. Abdul Mujeeb VM, Muraleedharan K, Kannan MP, Devi TG. Influence of trivalent ion dopants on the thermal decomposition kinetics of potassium bromate. Thermochim Acta (submitted).
42. Abdul Mujeeb VM, Aneesh MH, Muraleedharan K, Devi TG, Kannan MP. Effect of precompression on isothermal decomposition kinetics of potassium bromate. J Therm Anal Calorim. doi: 10.1007/s10973-010-1127-8.
43. Kannan MP, Muraleedharan K. Kinetics of thermal decomposition of sulphate-doped potassium metaperiodate. Thermochim Acta. 1990;158:259–66.
44. Vyazovkin S, Wight CA. Kinetics in solids. Annu Rev Phys Chem. 1997;48:125–49.
45. Kenneth S, editor. Principles of solid-state chemistry. Reactions in solids. London: MacLaren & Sons Ltd.; 1968. p. 21.
46. Muraleedharan K, Kannan MP, Ganga Devi T. Thermal decomposition kinetics of potassium iodate. J Therm Anal Calorim. 2011;103:943–55.
47. Philips BR, Taylor O. Thermal decomposition of potassium metaperiodate. J Chem Soc 1963:5583–90.
48. Muraleedharan K, Kannan MP. Effects of dopants on the isothermal decomposition kinetics of potassium metaperiodate. Thermochim Acta. 2000;359:161–8.

49. Muraleedharan K, Kannan MP, Gangadevi T. Effect of metal oxide additives on the thermal decomposition kinetics of potassium metaperiodate. J Therm Anal Calorim. 2010;100:177–82.
50. Muraleedharan K, Kannan MP, Gangadevi T. Thermal decomposition of potassium metaperiodate doped with trivalent ions. Thermochim Acta. 2010;502:24–9.
51. Markovitz MM, Boryta DA. The decomposition kinetics of lithium perchlorate. J Phys Chem. 1961;65:1419–24.
52. Kim S, Kavitha D, Yu TU, Jung JS, Song JH, Lee SW, Kong SH. Using isothermal kinetic results to estimate kinetic triplet of pyrolysis reaction of polypropylene. J Anal Appl Pyro. 2008;81:100–5.
53. Nakamura H, Sakumoto K, Hara Y, Ochi K. Thermal analysis of sodium azide. J Hazard Mater. 1994;38:1–12.
54. Bircumshaw LL, Newman BH. The thermal decomposition of ammonium perchlorate II. The kinetics of the decomposition, the effect of particle size, and discussion of results. Proc Roy Soc Lond. 1955;A227:228–41.
55. Pai Verneker VR, Kishore K, Kannan MP. Effect of pretreatment on the sublimation of ammonium perchlorate. J Appl Chem Biotechnol. 1977;27:309–17.
56. Maycock JN, Pai Verneker VR, Rouch L Jr. Influence of growth parameters on the reactivity of ammonium perchlorate. Inorg Nucl Chem Lett. 1968;4:119–23.
57. Boldyrev VV, Avvakumov L. Mechanochemistry of inorganic solids. Russ Chem Rev. 1971;40:847–59.
58. Pai Verneker VR, Maycock JN. The thermal decomposition of ammonium perchlorate at low temperature. J Inorg Nucl Chem. 1967;29:2723–30.
59. Mitchell JW, DeVries RC, Roberts RW, Cynon P, editors. Reactivity of solids. New York: Wiley-Interscience; 1969. p. 287.
60. Muraleedharan K, Abdul Mujeeb VM, Aneesh MH, Ganga Devi T, Kannan MP. Effect of pre-treatments on isothermal decomposition kinetics of potassium metaperiodate. Thermochim Acta. 2010;510:160–7.
61. Huang Y, Risha GA, Yang V, Yetter RA. Effect of particle size on combustion of aluminum particle dust in air. Combust Flame. 2009;156:5–13.
62. Chou CJ, Olsen FA. Isothermal decomposition of isothiocyanatopentaamine cobalt(III) perchlorate. Particle size effect. Anal Chem. 1972;44:1841–4.